Local electronic state in the half-metallic ferromagnet CrO_2 investigated by site-selective ^{53}Cr NMR measurements

Hikaru Takeda,[1,*] Yasuhiro Shimizu,[1] Yoshiaki Kobayashi,[1] Masayuki Itoh,[1] Takaaki Jin-no,[2] Masahiko Isobe,[3] Yutaka Ueda,[4] Sho Yoshida,[5,6] Yuji Muraoka,[5,6] and Takayoshi Yokoya[5,6]

[1]*Department of Physics, Graduate School of Science, Nagoya University, Furo-cho, Chikusa-ku, Nagoya 464-8602, Japan*

[2]*Technical Center, Nagoya University, Furo-cho, Chikusa-ku, Nagoya 464-8601, Japan*

[3]*Max Plank Institute for Solid State Research, Heisenbergstrasse 1, 70569, Stuttgart, Germany*

[4]*Toyota Physical and Chemical Research Institute, 41-1 Yokomichi, Nagakute, Aichi 480-1192, Japan*

[5]*Graduate School of Natural Science and Technology, Okayama University, 3-1-1 Tsushima-naka, Kita-ku, Okayama 700-8530, Japan*

[6]*Research Laboratory for Surface Science, Faculty of Science, Okayama University, 3-1-1 Tsushima-naka, Kita-ku, Okayama 700-8530, Japan*

(Received 15 February 2016; revised manuscript received 1 May 2016; published 15 June 2016)

We have made ^{53}Cr NMR measurements on polycrystalline and single-crystalline film samples to study the local electronic state of a half-metallic ferromagnet CrO_2 which has the rutile structure with one crystallographically equivalent Cr site. We observe two kinds of ^{53}Cr NMR spectra in the ferromagnetic state of both the samples. An analysis on the hyperfine field shows the presence of two Cr sites with different orbital occupancies, suggesting that a local orbital order takes place with breaking the local symmetry in the rutile structure. This may be ascribed to the negative charge transfer between chromium and oxygen ions.

DOI: 10.1103/PhysRevB.93.235129

I. INTRODUCTION

$3d$ transition metal oxides in the charge transfer regime have a peculiar electronic state resulting from the strong hybridization between transition-metal $3d$ and oxygen $2p$ orbitals [1,2]. These systems prefer to create a hole on the oxygen ions to avoid unstable high valence of transition metal ions. Then, the hole introduced into the p band by chemical substitution provides intriguing phenomena such as a Zhang-Rice singlet which plays a crucial role for high-T_c superconductivity in cuprates, an electronic phase separation leading to the giant magnetoresistance (GMR) in manganese oxides, and an intermediate spin state in cobaltite oxides [1–4].

Recently, high-valence chromium oxides in the negative-charge transfer regime have attracted attention as one of such systems. An itinerant ferromagnet $K_2Cr_8O_{16}$ with the quasi-one-dimensional (quasi-1D) Hollandite-type structure undergoes an unconventional metal-insulator (MI) transition with maintaining the ferromagnetic (FM) state. This is ascribed to the Peierls-like instability of the quasi-1D electronic structure due to the strong $3d$ and $2p$ hybridization forming a tunnel with a Cr tetramer as a structural unit [5–14]. A semiconducting antiferromagnet $NaCr_2O_4$ exhibits the GMR effect in the antiferromagnetic (AFM) phase, which is quite a contrast to the GMR effect conventionally observed in the FM phase of manganese oxides, for example [15–18]. An anomalous electronic state is discussed to come from the self-doping due to the negative charge transfer in a typical high-valence chromium oxide CrO_2 [19–21].

CrO_2 ($3d^2$), a half-metallic ferromagnet with the Curie temperature $T_C = 394$ K, is crystallized into the rutile structure (space group $P4_2/mnm$) [22] with one crystallographically equivalent Cr site presented in Fig. 1. First principles calculations in a local spin-density approximation (LSDA) revealed the band structure in the FM state [20,21]. One t_{2g} electron predominantly occupies the narrow majority d_{xy} band, wheras broad $d_{yz\pm zx}$ bands are partially occupied, resulting in localized character of d_{xy} electron and relatively itinerant character of $d_{yz\pm zx}$. This leads to the double exchange-type transfer hopping generating an FM interaction similar to $K_2Cr_8O_{16}$. CrO_2 has been extensively investigated for various aspects such as a negative-charge transfer oxide [2,3,20] or a potential candidate for spintronics due to the nearly full spin polarization of conduction electrons [23–29]. Recently, based on ^{53}Cr nuclear magnetic resonance (NMR) measurement of a polycrystalline CrO_2 sample, Shim *et al.* proposed that there are two Cr sites with different spontaneous moments in spite of one crystallographic Cr site [30]. They discussed the valence state of $Cr^{+4\pm\delta}$ due to the self-doping, lattice distortion, and very slow charge fluctuations owing to the charge transfer process from oxygen ions as its origin. However, the electronic state and the origin have not been well elucidated from the microscopic point of view. A similar phenomenon was observed in our ^{53}Cr NMR measurements on $K_2Cr_8O_{16}$ in the FM metallic phase with the tetragonal structure above the MI transition where the structural transition occurs simultaneously [14]. Since both the oxides have a similar four-chain column along the c axis as a structural unit [Fig. 1(a)], they may have a common feature due to the negative charge transfer. Thus it is valuable to elucidate the origin of the anomalous electronic state in CrO_2 with no structural transition. Recently, we have developed the orbital-resolved NMR method to study the orbital state in multiorbital $3d$ electron systems [31–34]. This is a useful method to clarify the orbital state in CrO_2.

In this study we have made ^{53}Cr NMR measurements on polycrystalline and single crystalline-film samples of CrO_2. We observe two sets of ^{53}Cr spectra coming from a single domain in the FM phase of both the samples. An analysis of the internal fields at the two Cr sites based on the orbital-resolved

*Present address: Institute for Solid State Physics, University of Tokyo, 5-1-5 Kashiwanoha, Kashiwa, Chiba 277-8581, Japan.

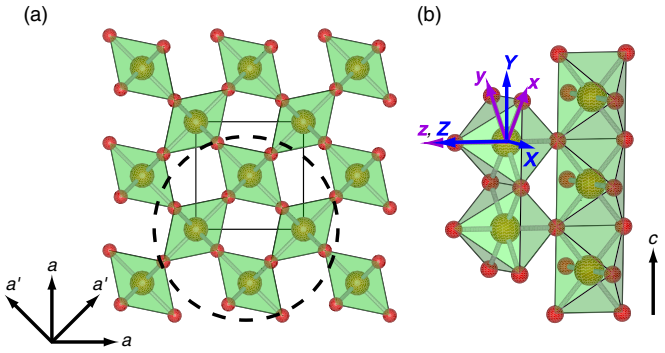

FIG. 1. (a) Crystal structure of CrO_2 projected on the c plane. The square represents a unit cell, whereas the dashed circle denotes a four-chain column along the c axis as a structural unit. (b) Chains composed of edge shared CrO_6 octahedra with the local x, y, and z axes and the principal X, Y, and Z ones of the ^{53}Cr hyperfine coupling tensor.

NMR technique enables us to investigate the electronic state in CrO_2. We find that the two Cr sites do not have different valence states but $3d$ orbital occupation numbers different from each other. Such a peculiar electronic state may be ascribed to the orbital-dependent charge transfer which induces a local orbital order.

II. EXPERIMENTAL PROCEDURE

The polycrystalline sample of CrO_2 used in this study was a commercial product (Kojundo Kagaku), whereas the (100)-oriented single crystalline film on TiO_2 (100) substrate with the size of $5 \times 3 \times 0.5$ mm^3 was prepared by a chemical vapor deposition technique as reported in Ref. [25]. The thickness of the film is estimated as ~300 nm and $\sim 1.6 \times 10^{17}$ ^{53}Cr nuclei are contained in the film. Although this number of the nuclei is about 2×10^3 times smaller than that in the polycrystalline sample of 50 mg, we could detect the NMR signal due to the enhancement effect in ferromagnets. The shape of the polycrystalline sample was analyzed by a scanning electron microscope (SEM, Hitachi High-Technologies, S-4800). Magnetization measurements on the film were made by using a superconducting quantum interface device (SQUID) magnetometer (Quantum Design, MPMS). ^{53}Cr NMR measurements were performed by a conventional pulse technique, and Fourier-transformed (FT) NMR spectra of a spin-echo signal were obtained at various external fields. The ^{53}Cr nucleus has a nuclear spin $I = 3/2$ and the gyromagnetic ratio $\gamma_n = 2\pi \times 2.406$ MHz/T.

Before presenting our experimental results, it is useful to summarize characteristic features of an NMR spectrum in an FM state [35–37]. In general, spontaneous magnetic moments $\mathbf{M}$ generate an internal magnetic field $\mathbf{H}_n$ expressed as $\mathbf{H}_n = \mathbf{H}_{hf} + \mathbf{H}_D + \mathbf{H}_{demag} + \mathbf{H}_L$ with the hyperfine field $\mathbf{H}_{hf}$, the classical dipole one $\mathbf{H}_D$, the demagnetization one $\mathbf{H}_{demag}$, and the Lorentz one $\mathbf{H}_L$ at a nucleus in the FM phase [37]. This enables us to observe the NMR spectrum even under zero external field $\mathbf{H}_0 = 0$. Then we can detect the NMR signals from nuclei in magnetic domains and domain walls with a strong enhancement effect. The domain signal forms a relatively narrow spectrum which depends on the multidomain structure, whereas the domain-wall one forms a so-called powder pattern due to the spontaneous moments rotated in the domain walls. If $\mathbf{H}_n$ at the nuclei in a 180° wall are rotated continuously in a plane, we can observe a two-dimensional (2D) powder pattern with a double-horn structure. Application of external field removes the walls and changes the multidomain state to a single domain one above the saturation field H_s where magnetization saturates. Then, in a polycrystalline sample the NMR spectral shape changes by applying H_0. As observed in a ferromagnet $K_2Cr_8O_{16}$, the 2D powder pattern coming from the domain wall gradually weakens and vanishes above H_s [14]. The domain spectrum changes from the relatively sharp spectrum to the three-dimensional (3D) powder pattern with three singularities at resonance frequencies $\nu = \frac{\gamma_n}{2\pi}|H_0 + H_n^k|$ ($k = X, Y$, and Z), where H_n^k is the principal k component of $\mathbf{H}_n$, above H_s [14]. Also we define the isotropic internal field $H_n^{iso} = (H_n^X + H_n^Y + H_n^Z)/3$, the axially anisotropic one $H_n^{ax} = (2H_n^Z - H_n^Y - H_n^X)/6$, and the in-plane anisotropic one $H_n^{aniso} = (H_n^Y - H_n^X)/2$. In a single crystalline film, ν for a domain obeys a resonance condition $\nu = \frac{\gamma_n}{2\pi}|\mathbf{H}_0 + \mathbf{H}_n|$, where $\mathbf{H}_n$ complicatedly changes with the reorientation of $\mathbf{M}$ under an external field.

III. EXPERIMENTAL RESULTS AND ANALYSIS

A. Polycrystal

The polycrystalline CrO_2 sample used in this study is an ensemble of needlelike ones with a length of 200–600 nm and a diameter of ~20 nm as seen in the SEM image shown in the inset of Fig. 2. Figure 2 presents the ^{53}Cr NMR spectra of the polycrystalline CrO_2 at 4.2 K under various external fields of $H_0 = 0$, 0.3, 0.4, and 0.5 T. At zero field, we observed two sharp spectra, CrA and CrB, at 26.5 and 37.2 MHz with full width at half maximum (FWHM) of 0.45 and 0.68 MHz, respectively, consistent with the previous NMR results [30,38]. The quadrupole splitting caused by a noncubic electric field gradient at the ^{53}Cr nucleus would be hidden in the spectrum width [14]. These sharp linewidths imply that the spectra are

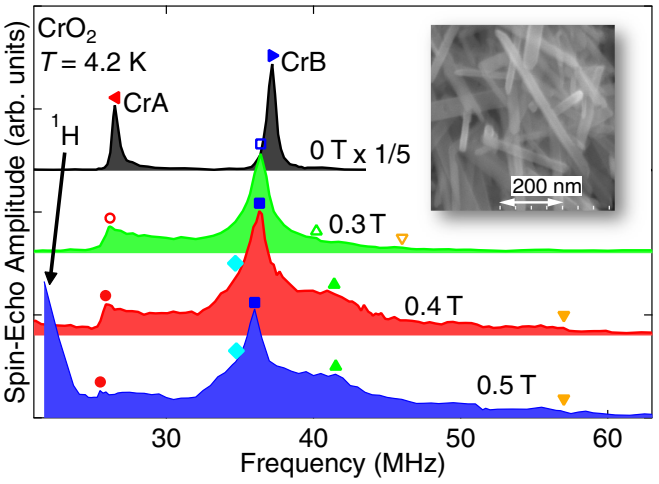

FIG. 2. ^{53}Cr NMR spectra of the polycrystalline CrO_2 at 4.2 K under various magnetic fields. The inset shows a SEM image and the symbols represent singularity points in the NMR spectra. The ^{1}H spectrum comes from ^{1}H nuclei outside the sample.

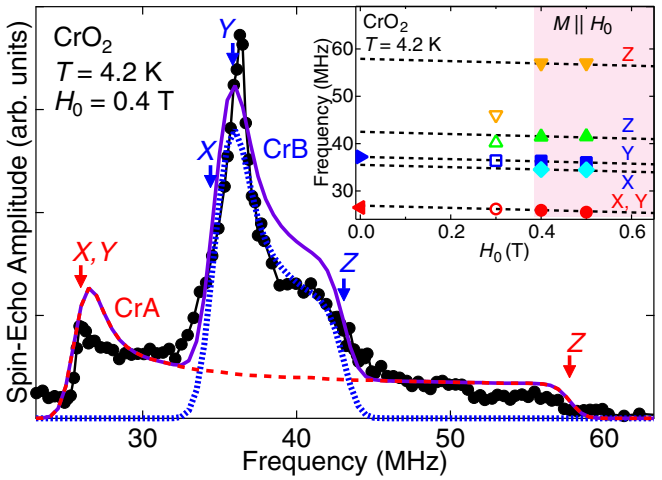

FIG. 3. ^{53}Cr NMR spectrum of the polycrystalline CrO_2 at 4.2 K and 0.4 T with the powder patterns, CrA and CrB, calculated for the internal fields listed in Table I. The purple curve is the summation of the two powder patterns. The inset shows NMR frequency versus H_0 for $H_0 \parallel k$ ($k = X$, Y, and Z) above 0.4 T and the singularity points marked in Fig. 2 below 0.3 T. The dashed lines represent $\nu = \frac{\gamma_n}{2\pi}(-H_n^k - H_0)$ with the H_n^k values listed in Table I.

more likely to come from a magnetic domain as discussed in the previous report [30]. The NMR signals from the domain walls are too small to be detectable, since a multidomain structure cannot be formed in the present small grain sample with the small diameter comparable to a domain size [29].

With increasing H_0, the zero-field NMR spectrum with two peaks turns to a powder pattern with peaks and steps. Above 0.4 T where magnetization nearly saturates, the NMR spectrum turns to a broad spectrum measured at an interval of two pulses $\tau = 60\,\mu$s. A correction due to the nuclear spin-spin relaxation time T_2 is not made in this spectrum, since the τ value is much shorter than the T_2 values of 4.0 (3.3) ms at 26.0 (36.3) MHz obtained by fitting the experimental data of the spin-echo intensity $I(\tau)$ to $I(\tau) = I(0)\exp(-2\tau/T_2)$. Because of the high frequency resolution and the signal to noise ratio in the present spectrum compared to the previous studies [30,38], we can decompose the spectrum to two sets of 3D powder patterns. As seen in Fig. 3, the experimental spectrum at 0.4 T can be well reproduced by the superposition of the two randomly oriented 3D powder patterns, CrA and CrB, calculated for the values of H_n^k ($k = X$, Y, and Z) listed in Table I. In this calculation we assume the same intensity for CrA and CrB, and take convolution of a Gaussian with FWHM of 2.0 MHz. With increasing H_0 above 0.4 T, the NMR frequencies for $H_n \| k$ obey the relation $\nu = \frac{\gamma_n}{2\pi}(-H_n^k - H_0)$ with the H_n^k values listed in Table I as seen in the inset of Fig. 3. In the inset, frequencies for $H_n \parallel k$ in a single domain above 0.4 T, those for the singularities in the spectrum at 0.3 T, and those for the peaks in the zero-field spectrum are presented as the NMR frequency. This shows that $\mathbf{H}_n$ has a negative hyperfine coupling constant mainly governed by the core polarization effect and the sample sets in a single domain state with $\mathbf{M} \parallel \mathbf{H}_0$ above 0.4 T. Furthermore, a fact that the NMR frequencies at zero field follow the equations for $k = Y$ means that the Y axis is the easy axis. Taking into account that the easy axis is along the c direction [28,29,39], Y is parallel to c whereas X and Z are in the c plane. This is consistent with the local symmetry of the Cr site, $m.mm$, with three mirror planes normal to the c and a' axes where the a' axis is located at 45° tilted from the a axis in the c plane as shown in Fig. 1(a) [22]. Also the X, Y, and Z axes, which are governed by $\mathbf{H}_{hf}$, in CrO_2 would be approximately parallel to the local symmetry axes, $x - y$, $x + y$, and z, respectively, as seen in Fig. 1(b).

TABLE I. Principal components and their errors of the internal field H_n^k ($k = X$, Y, and Z) for the Cr NMR spectra, CrA and CrB, in CrO_2.

Spectrum	H_n^X (T)	H_n^Y (T)	H_n^Z (T)
CrA	-11.2 ± 0.2	-11.2 ± 0.2	-24.4 ± 0.3
CrB	-14.7 ± 0.2	-15.3 ± 0.2	-18.3 ± 0.3

Thus it is confirmed that the sharp NMR spectra at zero field come from domains comparable in size to the nanoscale needle which may be a small single crystal with $\mathbf{M}$ parallel to the c axis (the needle axis) [29]. We can conclude that there are two Cr sites which have almost equal volume fractions and the different internal fields in CrO_2.

B. Single crystalline film

Figure 4 shows magnetization M_α versus H_0 for the single-crystalline CrO_2 film measured at 4.2 K with H_0 applied along the α ($= a$, b, and c) direction which is introduced to identify the sample shape. The b direction is parallel to the a axis in the film plane, whereas the a one is along another a axis perpendicular to the plane. M_c parallel to the easy c axis raises abruptly with increasing H_0, whereas M_a and M_b parallel to the hard one increase more slowly with increasing H_0. It should be noted that M_a has to trace M_b after correcting a nonzero $\mathbf{H}_{demag}$.

As presented in Fig. 5, two ^{53}Cr NMR spectra, CrA and CrB, with FWHM of 0.19 and 0.28 MHz were observed at 26.7 and 37.7 MHz, respectively, in the zero-field NMR spectrum of the single-crystalline film at 4.2 K. These come from domains with

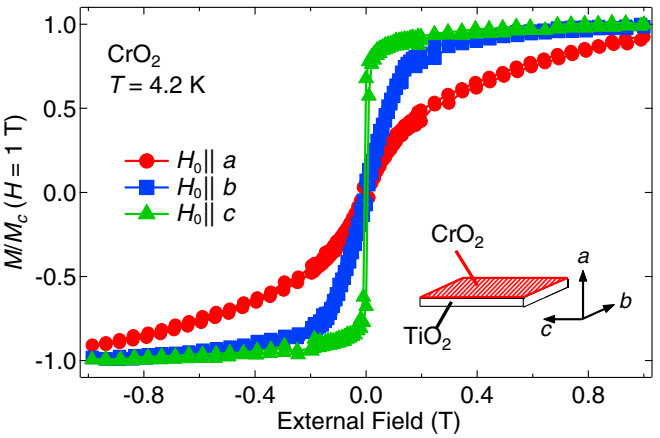

FIG. 4. Magnetization versus external magnetic field at 4.2 K with H_0 applied along the a, b, and c directions for the single-crystalline CrO_2 film. Magnetization is normalized against M_c at 1 T. The inset is a schematic figure of the film.

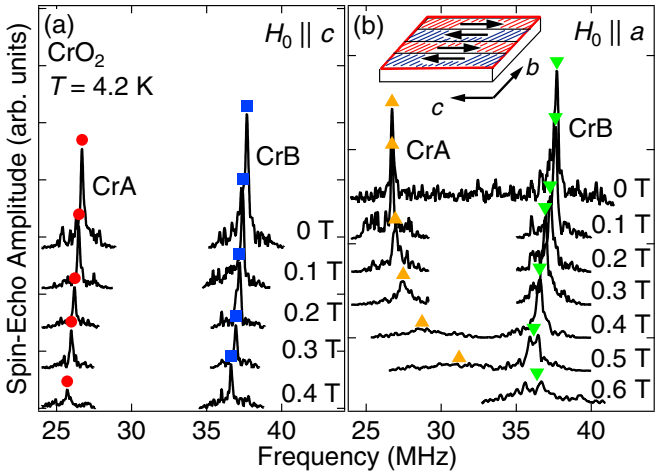

FIG. 5. ^{53}Cr NMR spectra at 4.2 K with H_0 applied along the (a) c and (b) a directions in the single-crystalline CrO_2 film. The inset shows a schematic domain structure at zero field.

$\mathbf{M} \parallel \mathbf{c}$ in the film plane as schematically represented in the inset of Fig. 5, whereas spectra from few walls may be too small to be detectable. The ^{53}Cr NMR spectra at 4.2 K under various external fields are also presented in Fig. 5, where H_0 is applied to the a and c directions. The two peaks in the spectra for $H_0 \parallel c$ shift to lower frequencies with increasing H_0 after the domain walls are completely removed at 0.02 T as presented in Fig. 6(a). Concomitantly, the signal intensity decreases due to the suppression of the signal enhancement effect and the signals vanish above ~0.5 T. In the spectra for $H_0 \parallel a$, the peak of CrB shifts to a lower frequency up to ~0.5 T and slightly turns to a higher frequency with further increasing H_0, whereas the peak of CrA is almost H_0 independent at low fields and rapidly shifts to a higher frequency above ~0.2 T as seen in Fig. 6(b).

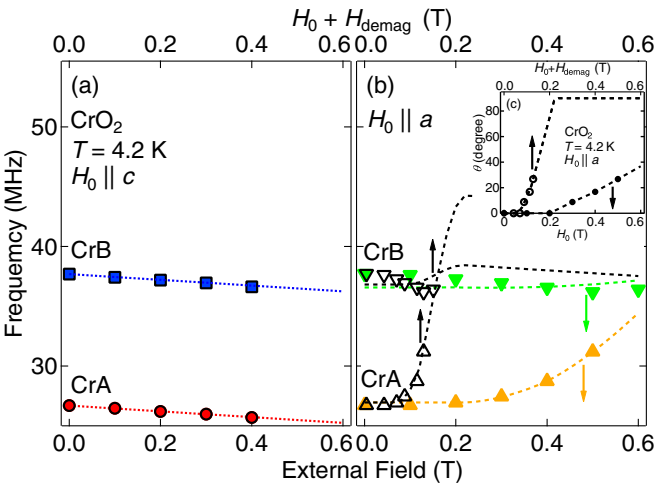

FIG. 6. ^{53}Cr NMR frequency versus H_0 for (a) $H_0 \parallel c$ and (b) $H_0 \parallel a$ at 4.2 K in the single-crystalline CrO_2 film. The dotted lines and dashed curves represent the calculated ones based on the resonance condition $f_{res} = \frac{\gamma_n}{2\pi}|\mathbf{H}_0 + \mathbf{H}_n|$ (see the text). The inset shows the H_0 dependence of the rotation angle of $\mathbf{M}$ from the c to a axes for $H_0 \parallel a$. Refer to the upper axes for the open symbols which are obtained after a demagnetization correction.

In an FM state, the demagnetization effect and the complicated evolution from multidomains to a single domain with increasing H_0 generally prevent us from analyzing the H_0 dependence of ν below H_s. However, the experimental results of the single-crystalline CrO_2 film are explained as mentioned in the following. For $H_0 \parallel c$, reasonably $\mathbf{H}_{demag} = 0$ and ν obey the relation $\nu = \frac{\gamma_n}{2\pi}(-H_n^c - H_0)$ with $-\gamma H_n^c/2\pi = 26.7$ (37.7) MHz for CrA (CrB) as represented by the red (blue) dotted line in Fig. 6(a). This behavior is consistent with the polycrystalline result. On the other hand, for $H_0 \parallel a$, we have to take account of nonzero $\mathbf{H}_{demag}$ which can be numerically obtained from comparing M_a with M_b in Fig. 4. Then, ν can be expressed as $\nu = \frac{\gamma_n}{2\pi}|\mathbf{H}_0 + \mathbf{H}_n|$, where $\mathbf{H}_n = \mathbf{AM}$ with the effective coupling tensor $\mathbf{A}$. Since the direction of $\mathbf{M}$ is governed by the effective magnetic field composed of the exchange field, the anisotropic field, $\mathbf{H}_0$, and so on, ν evolves complicatedly with increasing $\mathbf{H}_0$ along the hard axis. Assuming that the rotation angle θ of $\mathbf{M}$ evolves from the c axis in an external field as shown in the inset of Fig. 6(b), we can almost reproduce the experimental results for the H_0 dependence of ν for CrA and CrB as represented by the orange and green dashed curves, respectively, in Fig. 6(b) where the upper axis is introduced to make a correction due to H_{demag}. The slight deviation, which is especially noticeable in CrB, may come from more complex behavior of the spontaneous moments than we expect during the walls being removed. The curves are numerically calculated with the k ($= X$, Y, and Z) components of the $\mathbf{A}$ tensor obtained from the H_n^k values of the polycrystalline sample in Table I and $M = 2\mu_B$. As seen in the inset of Fig. 6(b), the H_0 dependence of the rotation angle of $\mathbf{M}$ obtained after the correction indicates that H_0 overcomes the anisotropic field above ~0.2 T.

In the (100)-oriented film grown on TiO_2 with thickness less than ~10 nm, the crystal structure is affected by the compressive strain along the out-of-plane and the tensile one along in-plane directions [40–42]. However, the present film with thickness of ~300 nm is considered to show almost the same properties as those of a bulk single crystal [25,39]. This is consistent with the present NMR results. Thus we can clearly conclude that there are two Cr sites, whose volume fractions are almost equal to each other, with $\mathbf{H}_n$ listed in Table I in both the polycrystalline and single-crystalline film samples of CrO_2.

IV. DISCUSSION

As mentioned above, there exist two kinds of Cr sites with different electronic states in spite of only one Cr site from the crystallographical point of view in CrO_2. Based on the internal field obtained in the present NMR experiments, we discuss the anomalous electronic state which breaks the lattice symmetry.

In general, the hyperfine field, which governs $\mathbf{H}_n$, is expressed as $\mathbf{H}_{hf} = \mathbf{H}_{hf}^{on} + \mathbf{H}_{STH}$, where $\mathbf{H}_{hf}^{on}$ is the hyperfine field on the Cr site and $\mathbf{H}_{STH}$ is the supertransferred hyperfine (STH) field. Then $\mathbf{H}_{hf}^{on}$ is composed of the isotropic Fermi contact field via the core polarization effect $\mathbf{H}_{cp} = -\kappa \langle r^{-3} \rangle \mathbf{M}$ and the anisotropic dipole hyperfine field, $\mathbf{H}_{dip} = -\sum_j \frac{2}{21} \langle r^{-3} \rangle f_j \mathbf{q}_j \mathbf{M}$ [43,44]. Here, κ is a parameter of the Fermi contact interaction, $\langle r^{-3} \rangle$ is an expectation value of r^{-3}

for the $3d$ orbitals, f_j is the fraction of the electron number for the d_j ($j = xy$ and $yz \pm zx$) orbital and $\Sigma_j f_j = 1$, and $\mathbf{q}$ is the electron quadrupole tensor $q_{\alpha\beta} = \frac{3}{2}(l_\alpha l_\beta + l_\beta l_\alpha) - \delta_{\alpha\beta}\mathbf{l}^2$ ($\alpha = x$, y, and z) with the orbital momentum $\mathbf{l}$. Thus we can obtain information on the orbital occupation from the isotropic and anisotropic components of $\mathbf{H}_{\rm hf}^{\rm on}$.

In order to obtain $\mathbf{H}_{\rm hf}^{\rm on}$ from $\mathbf{H}_{\rm n}$, we first evaluate $\mathbf{H}_{\rm demag}$, $\mathbf{H}_{\rm L}$, $\mathbf{H}_{\rm D}$, and $\mathbf{H}_{\rm STH}$. By assuming that $\mathbf{H}_{\rm demag} = -2\pi\mathbf{M}$ (zero) with $M = 2.0\,\mu_{\rm B}$ for $\mathbf{H}_0$ perpendicular (parallel) to the needle axis, we can obtain $-0.41\ {\rm T} \leqslant H_{\rm demag} \leqslant 0$. We also obtain $H_{\rm L} = 0.27$ T from $\mathbf{H}_{\rm L} = \frac{4\pi}{3}\mathbf{M}$. $\mathbf{H}_{\rm D}$ can be calculated as $H_{\rm D}^{\rm ax} = 0.046$ T and $H_{\rm D}^{\rm aniso} = 0.033$ T by taking summation over the lattice points with M in the Lorentz sphere, where the definitions of $H_{\rm D}^{\rm ax}$ and $H_{\rm D}^{\rm aniso}$ follow those of $H_{\rm n}^{\rm ax}$ and $H_{\rm n}^{\rm aniso}$. $\mathbf{H}_{\rm STH} = \Sigma_j \mathbf{B}_j \mathbf{M}_j$, which arises via Cr − O − Cr spin transfer processes from eight neighboring magnetic Cr sites with $\mathbf{M}$ [45–52], can be evaluated by assuming an isotropic STH coupling constant $B = 1.46$–$4.58\ {\rm T}/\mu_{\rm B}$ as discussed in Ref. [14]. After subtracting $\mathbf{H}_{\rm demag}$, $\mathbf{H}_{\rm L}$, $\mathbf{H}_{\rm D}$, and $\mathbf{H}_{\rm STH}$ from the experimental results listed in Table I, we can obtain values of $\mathbf{H}_{\rm hf}^{\rm on}$. Then the anisotropic components of $\mathbf{H}_{\rm hf}^{\rm on}$ provide the orbital occupation of $3d$ electrons as demonstrated in our previous NMR studies on vanadium and chromium oxides [31–34]. The ratios of the axially and in-plane anisotropic parts of $\mathbf{H}_{\rm dip}$ to $H_{\rm cp}$ are expressed as $H_{\rm dip}^{\rm ax}/H_{\rm cp} = \frac{1}{7\kappa}(2f_{xy} - f_{yz+zx} - f_{yz-zx})$ and $H_{\rm dip}^{\rm aniso}/H_{\rm cp} = \frac{3}{7\kappa}(f_{yz+zx} - f_{yz-zx})$, respectively. Comparing these equations with the experimental ones, we can obtain the electron number of each orbital, $n_j = nf_j$ where n is the total electron number at the Cr site in concern. The electron number, namely the Cr valence, is related to the magnetic moment generating $H_{\rm n}^{\rm iso}$. If the CrA and CrB sites may be occupied by $Cr^{+4\pm\delta}$ ($n = 2\mp\delta$) with magnetic moments of $n\mu_{\rm B}$ due to the self-doping proposed by Shim *et al.* [30], the ratio of $H_{\rm n}^{\rm iso}({\rm CrB})/H_{\rm n}^{\rm iso}({\rm CrA}) = 1.03$ provides a value of $\delta = 0.03$ much smaller than their estimated value of $\delta = 1/3$. This small δ value seems to show the negligible difference in valence between the CrA and CrB sites. Thus by assuming $n = 2$, n_j for each orbital is obtained for the CrA and CrB sites as listed in Table II. Here we used $\kappa = 0.5$, a typical value for the t_{2g} systems.

As seen in Table II, the d_{xy} orbital at the CrA site forming the CrA spectrum is nearly occupied by one $3d$ electron, while the CrB site has the d_{xy} occupation number smaller than that of the CrA site. According to the first principles calculation in LSDA, one electron occupies the polarized d_{xy} band with a relatively narrow band width, and broad $d_{yz\pm zx}$ ones, which cross the Fermi level, are occupied by another electron in the ferromagnetic state. Then, the observed difference in the electron number between the CrA and CrB sites seems to provide no effect on the double-exchange mechanism for the ferromagnetic interaction, since the orbital occupation of d_{xy} is larger than the others. Thus we can conclude that the two Cr sites have different orbital occupations, resulting in the electronic state which breaks the local symmetry of the rutile structure. The two types of the orbital occupations usually require a lattice-symmetry change, which may lead to the difference between the body-center and corner Cr sites, due to the coupling between the orbital degrees of freedom and the lattice. Although such a change has not been observed by conventional x-ray and neutron powder diffraction measurements [22,53,54], the atomic pair distribution function (PDF) analysis of the powder neutron scattering data recently indicated that the lowering of the lattice symmetry in a short-range scale takes place with the rutile structure as the average one [55]. If not so, there may be the lowering not detectable by the powder diffraction measurements. Then a synchrotron x-ray diffraction measurement on a CrO_2 single crystal is necessary to clarify whether it occurs or not.

TABLE II. Electron number of each d_j ($j = xy$ and $yz \pm zx$) orbital in CrO_2.

Spectrum	n_{xy}	n_{yz+zx}	n_{yz-zx}
CrA	0.78–0.93	0.54–0.61	0.53–0.61
CrB	0.69–0.73	0.65–0.66	0.62–0.65

The large difference in orbital occupancy at the two Cr sites and the slight lattice distortion seem to come from an electronic origin due to the negative charge transfer in CrO_2. In the high-valence chromium oxide $K_2Cr_8O_{16}$, the quasi-1D electronic structure governed by the negative charge transfer is known to provide the Peierls instability leading to the MI transition accompanied by a slight structural change from the tetragonal to monoclinic structures [9,11]. In CrO_2, there are two types of Cr-O bonds with different bond lengths of 0.1889 and 0.1913 nm [22]. Via the short bond, $2p$ electrons effectively transfer from an apical oxygen to its neighboring chromium due to the negative charge transfer process and the hybridization between the $d_{yz\pm zx}$ and oxygen p orbitals. In a similar process, another transition metal oxide in the negative charge transfer regime, $CaFeO_3$, exhibits a charge disproportionation transition with a lattice symmetry breaking [56]. Unlike this iron oxide, in CrO_2, the sufficiently broad band enables the ligand holes to be conductive and prohibits the system to undergo a charge order or a charge disproportionation transition. Nevertheless, the orbital-dependent charge transfer in CrO_2 may lead to an electronic structure which favors the orbital polarization accompanied by the slight lattice distortion in the short-range scale. In multiorbital systems, complex orbital-spin coupled interactions appear and result in various ground states. One example is an orbital-degenerated spin system where an orbital state is strongly coupled with the spin structure via the Kugel-Khomskii type interaction [57]. Similar type of interactions also exist in itinerant systems as discussed on iron pnictide superconductors [58,59]. In the case of itinerant systems, the orbital order is defined in terms of a different orbital occupation at different sites and an order parameter is orbital polarization [60]. Then, the difference in orbital occupancy, particularly notable for the d_{xy} orbital (see Table II) in CrO_2, may be ascribed to such a local orbital order associated with magnetic properties. More recently, it was reported that the origin of ferromagnetism in CrO_2 would be beyond the simple double exchange model [61]. Further-neighbor exchange interactions may compete with the dominant ferromagnetic interactions and may lead to instability of the double-exchange ferromagnetism in CrO_2.

An anomalous electronic state similar to that in CrO_2 appears in $K_2Cr_8O_{16}$ with $T_{\rm C} = 180$ K and $T_{\rm MI} = 95$ K, where the structural and MI transitions occur simultaneously [5–14].

We observed four sets of ^{53}Cr NMR spectra in the FM insulating phase with the monoclinic structure (space group $P112_1/a$) below T_{MI}, consistent with the presence of four crystallographically inequivalent Cr sites [14]. At least two sets were however observed even in the FM metallic phase with the tetragonal structure (space group $I4/m$) which has only one Cr site from the crystallographical point of view, although very weak NMR signals prevented us from studying the electronic state in detail. Both CrO_2 and $K_2Cr_8O_{16}$ have a similar structural unit of the four-chain column along the c axis as denoted in Fig. 1(a). The double-exchange process on the four-chain column plays an important role for the ferromagnetism of both the oxides [11]. The anomalous electronic states observed in the chromium oxides with the tetragonal structures seem to have the same origin due to the negative charge transfer as discussed above. The electronic state uncovered by the present NMR study of CrO_2 is an interesting issue on the 3d transition metal oxides in the negative charge regime and thus theoretical studies based on a microscopic model are desired to elucidate it.

V. CONCLUSION

We have made ^{53}Cr NMR measurements on polycrystalline and single crystalline samples to investigate the local electronic state in a half-metallic ferromagnet CrO_2 with only one crystallographic Cr site in the rutile structure. Two ^{53}Cr NMR spectra were observed in the ferromagnetic phase of both the samples. Based on the analysis of the internal field obtained from the single-domain NMR spectra, we found the presence of two Cr sites with different 3d orbital occupations. This suggests a local orbital order which conflicts with the local symmetry of the rutile structure. The anomalous electronic state may be related to the negative charge transfer.

ACKNOWLEDGMENTS

The authors would like to thank K. Kodama and Y. Ohta for fruitful discussion. This study was supported by the KAKENHI on Priority Area "Novel State of Matter Induced by Frustration" (Grant No. 22014006) from the Ministry of Education, Culture, Sports, Science, and Technology of Japan, and also the KAKENHI (Grants No. 24340080 and No. 25610092) from the Japan Society for the Promotion of Science (JSPS). One of the authors, H.T., was also supported by the Program for Leading Graduate Schools entitled "Integrative Graduate Education and Research Program in Green Natural Sciences" and the Grant-in-Aid for JSPS Fellows.

[1] M. Imada, A. Fujimori, and Y. Tokura, Rev. Mod. Phys. **70**, 1039 (1998).
[2] D. I. Khomskii, Lith. J. Phys. **37**, 65 (1997); see also arXiv:cond-mat/0101164, and references therein.
[3] D. I. Khomskii and G. A. Sawatzky, Solid State Commun. **102**, 87 (1997).
[4] E. Dagotto, Science **309**, 257 (2005).
[5] O. Tamada, N. Yamamoto, T. Mori, and T. Endo, J. Solid State Chem. **126**, 1 (1996).
[6] J. Sugiyama, H. Nozaki, M. Mansson, K. Prsa, D. Andreica, A. Amato, M. Isobe, and Y. Ueda, Phys. Rev. B **85**, 214407 (2012).
[7] K. Hasegawa, M. Isobe, T. Yamauchi, H. Ueda, J. I. Yamaura, H. Gotou, T. Yagi, H. Sato, and Y. Ueda, Phys. Rev. Lett. **103**, 146403 (2009).
[8] P. Mahadevan, A. Kumar, D. Choudhury, and D. D. Sarma, Phys. Rev. Lett. **104**, 256401 (2010).
[9] A. Nakao, Y. Yamaki, H. Nakao, Y. Murakami, K. Hasegawa, M. Isobe, and Y. Ueda, J. Phys. Soc. Jpn. **81**, 054710 (2012).
[10] M. Sakamaki, T. Konishi, and Y. Ohta, Phys. Rev. B **80**, 024416 (2009).
[11] T. Toriyama, A. Nakao, Y. Yamaki, H. Nakao, Y. Murakami, K. Hasegawa, M. Isobe, Y. Ueda, A. V. Ushakov, D. I. Khomskii, S. V. Streltsov, T. Konishi, and Y. Ohta, Phys. Rev. Lett. **107**, 266402 (2011).
[12] T. Yamauchi, K. Hasegawa, H. Ueda, M. Isobe, and Y. Ueda, Phys. Rev. B **92**, 165115 (2015).
[13] S. Kim, K. Kim, and B. I. Min, Phys. Rev. B **90**, 045124 (2014).
[14] H. Takeda, Y. Shimizu, M. Itoh, M. Isobe, and Y. Ueda, Phys. Rev. B **88**, 165107 (2013).
[15] H. Sakurai, T. Kolodiazhnyi, Y. Mihiue, E. Takayama-Muromachi, Y. Tanabe, and H. Kikuchi, Angew. Chem. Int. Ed. **51**, 6653 (2012).
[16] T. Kolodiazhnyi and H. Sakurai, J. Appl. Phys. **113**, 224109 (2013).
[17] H. Takeda, Y. Shimizu, M. Itoh, H. Sakurai, and E. Takayama-Muromachi, J. Korean Phys. Soc. **62**, 1914 (2013).
[18] A. Urushibara, Y. Moritomo, T. Arima, A. Asamitsu, G. Kido, and Y. Tokura, Phys. Rev. B **51**, 14103 (1995).
[19] K. Schwarz, J. Phys. F **16**, L211 (1986).
[20] M. A. Korotin, V. I. Anisimov, D. I. Khomskii, and G. A. Sawatzky, Phys. Rev. Lett. **80**, 4305 (1998).
[21] A. Toropova, G. Kotliar, S. Y. Savrasov, and V. S. Oudovenko, Phys. Rev. B **71**, 172403 (2005).
[22] T. J. Swoboda, P. Arthur, Jr., N. L. Cox, J. N. Ingraham, A. L. Oppegard, and M. S. Sadler, J. Appl. Phys. **32**, S374 (1961).
[23] Y. Ji, G. J. Strijkers, F. Y. Yang, C. L. Chien, J. M. Byers, A. Anguelouch, G. Xiao, and A. Gupta, Phys. Rev. Lett. **86**, 5585 (2001).
[24] J. S. Parker, S. M. Watts, P. G. Ivanov, and P. Xiong, Phys. Rev. Lett. **88**, 196601 (2002).
[25] K. Iwai, Y. Muraoka, T. Wakita, M. Hirai, T. Yokoya, Y. Kato, T. Muro, and Y. Tamenori, J. Appl. Phys. **108**, 043916 (2010).
[26] H. Fujiwara, M. Sunagawa, K. Terashima, T. Kittaka, T. Wakita, Y. Muraoka, and T. Yokoya, Appl. Phys. Lett. **106**, 202404 (2015).
[27] A. Biehler, M. Kläui, M. Fonin, C. König, G. Güntherodt, and U. Rüdiger, Phys. Rev. B **75**, 184427 (2007).
[28] X. Zou and G. Xiao, Appl. Phys. Lett. **91**, 113512 (2007).
[29] P. Das, F. Porrati, S. Wirth, A. Bajpai, M. Huth, Y. Ohno, H. Ohno, and J. Müller, Appl. Phys. Lett. **97**, 042507 (2010).

[30] J. H. Shim, S. Lee, J. Dho, and D.-H. Kim, Phys. Rev. Lett. **99**, 057209 (2007).
[31] Y. Shimizu, H. Takeda, M. Tanaka, M. Itoh, S. Niitaka, and H. Takagi, Nat. Commun. **3**, 981 (2012).
[32] Y. Shimizu, K. Matsudaira, M. Itoh, T. Kajita, and T. Katsufuji, Phys. Rev. B **84**, 064421 (2011).
[33] H. Takeda, M. Itoh, and H. Sakurai, Phys. Rev. B **86**, 174405 (2012).
[34] T. Kiyama, T. Shiraoka, M. Itoh, L. Kano, H. Ichikawa, and J. Akimitsu, Phys. Rev. B **73**, 184422 (2006).
[35] C. P. Slichter, *Principles of Magnetic Resonace* (Springer-Verlag, Berlin, 1990).
[36] A. C. Gossard and A. M. Portis, Phys. Rev. Lett. **3**, 164 (1959).
[37] W. Marshall, Phys. Rev. **110**, 1280 (1958).
[38] H. Nishihara, T. Tsuda, A. Hirai, and T. Shinjo, J. Phys. Soc. Jpn. **32**, 85 (1972).
[39] G. Miao, G. Xiao, and A. Gupta, Phys. Rev. B **71**, 094418 (2005).
[40] H. Sato, M. Pathak, D. Mazumdar, X. Zhang, G. J. Mankey, P. LeClair, and A. Gupta, J. Appl. Phys. **109**, 103907 (2011).
[41] M. Pathak, H. Sims, K. B. Chetry, D. Mazumdar, P. R. LeClair, G. J. Mankey, W. H. Butler, and A. Gupta, Phys. Rev. B **80**, 212405 (2009).
[42] M. Pathak, H. Sato, X. Zhang, K. B. Chetry, D. Mazumdar, P. R. LeClair, and A. Gupta, J. Appl. Phys. **108**, 053713 (2010).
[43] T. Kiyama and M. Itoh, Phys. Rev. Lett. **91**, 167202 (2003).
[44] A. Abragam and F. Bleany, *Electron Paramagnetic Resonance of Transition Ions* (Clarendon Press, Oxford, 1970).
[45] F. Mila and T. M. Rice, Physica C **157**, 561 (1989).
[46] T. Shimizu, H. Yasuoka, T. Tsuda, K. Koga, and Y. Ueda, Bull. Magn. Reson. **12**, 39 (1990).
[47] A. J. Freeman and R. E. Watoson, *Hyperfine Interaction* (Academic Press, New York, 1967).
[48] J. Kikuchi, H. Yasuoka, Y. Kokubo, Y. Ueda, and T. Ohtani, J. Phys. Soc. Jpn. **65**, 2655 (1996).
[49] F. van der Woude and G. A. Sawatzky, Phys. Rev. B **4**, 3159 (1971).
[50] A. S. Moskvin, N. S. Ovanesyan, and V. A. Trukhtanov, Hyperfine Interact. **3**, 429 (1977).
[51] I. A. Presniakov, V. S. Rusakov, G. Demazeau, A. V. Sobolev, Ya. S. Glazkova, T. V. Gubaidulina, A. M. Gapochka, O. S. Volkova, and A. N. Vasiliev, Phys. Rev. B **85**, 024406 (2012).
[52] A. K. Koh and D. F. Miller, At. Data Nucl. Data Tables **33**, 235 (1985).
[53] W. H. Cloud, D. S. Schreiber, and K. R. Babcock, J. Appl. Phys. **33**, 1193 (1962).
[54] J. Dho, S. Ki, A. F. Gubkin, J. M. S. Park, and E. A. Sherstobitova, Solid State Commun. **150**, 86 (2010).
[55] K. Kodama, K. Ikeda, M. Isobe, H. Takeda, M. Itoh, Y. Ueda, S. Shamoto, and T. Otomo (unpublished).
[56] S. Kawasaki, M. Takano, R. Kanno, T. Takeda, and A. Fujimori, J. Phys. Soc. Jpn. **67**, 1529 (1998).
[57] K. I. Kugel and D. I. Khomskii, Sov. Phys. Usp. **136**, 621 (1982).
[58] F. Krüger, S. Kumar, J. Zaanen, and J. van den Brink, Phys. Rev. B **79**, 054504 (2009).
[59] H. Kontani, T. Saito, and S. Onari, Phys. Rev. B **84**, 024528 (2011).
[60] E. Bascones, B. Valenzuela, and M. J. Calderón, Phys. Rev. B **86**, 174508 (2012).
[61] I. V. Solovyev, I. V. Kashin, and V. V. Mazurenko, Phys. Rev. B **92**, 144407 (2015).